A CellAgeClock for expedited discovery of anti-ageing compounds

Celia Lujan[1,*], Eleanor J. Tyler[2,*], Simone Ecker[3,*], Amy P. Webster[3,*], Eleanor R. Stead[1], Victoria E. Martinez Miguel[1], Deborah Milligan[2], James C. Garbe[4], Martha R. Stampfer[4], Stephan Beck[3,#], Robert Lowe[5,#], Cleo L. Bishop[2,#], Ivana Bjedov[1,#]

Affiliations

[1]: UCL Cancer Institute, Paul O'Gorman Building, University College London, 72 Huntley Street London, London WC1E 6DD, UK
[2]: Centre for Cell Biology and Cutaneous Research, Blizard Institute, Barts and The London School of Medicine and Dentistry, Queen Mary University of London, 4 Newark Street, London E1 2AT
[3]: Medical Genomics Group, UCL Cancer Institute, University College London, London WC1E 6BT, UK
[4]: Biological Systems and Engineering Division, Lawrence Berkeley National Laboratory, Berkeley, CA, United States
[5]: Centre for Genomics and Child Health, Blizard Institute, Barts and The London School of Medicine and Dentistry, Queen Mary University of London, 4 Newark Street, London E1 2AT

*Equal contribution
#corresponding authors:
i.bjedov@ucl.ac.uk c.l.bishop@qmul.ac.uk rlowe.compbio@gmail.com s.beck@ucl.ac.uk

Abstract

We aim to improve anti-ageing drug discovery, currently achieved through laborious and lengthy longevity analysis. Recent studies demonstrated that the most accurate molecular method to measure human age is based on CpG methylation profiles, as exemplified by several epigenetics clocks that can accurately predict an individual's age. Here, we developed CellAgeClock, a new epigenetic clock that measures subtle ageing changes in primary human cells *in vitro*. As such, it provides a unique tool to measure effects of relatively short pharmacological treatments on ageing. We validated the CellAgeClock against known longevity drugs such as rapamycin and trametinib. Moreover, we uncovered novel anti-ageing drugs, torin2 and Dactolisib (BEZ-235), demonstrating the value of our approach as a screening and discovery platform for anti-ageing strategies. The CellAgeClock outperforms other epigenetic clocks in measuring subtle ageing changes in primary human cells in culture. The tested drug treatments reduced senescence and other ageing markers, further consolidating our approach as a screening platform. Finally, we show that the novel anti-ageing drugs we uncovered *in vitro,* indeed increased longevity *in vivo*. Our method expands the scope of CpG methylation profiling from measuring human chronological and biological age from human samples in years, to accurately and rapidly detecting anti-ageing potential of drugs using human cells *in vitro*, providing a novel accelerated discovery platform to test sought after geroprotectors.

One of the remarkable achievements of developed countries is a continuous increase in life expectancy at birth, leading to greater longevity. However, a higher proportion of elderly in modern societies is accompanied by a steep increase in people suffering from age-related diseases. For example, cancer incidence rates, currently at 17 million worldwide, are expected to increase to 26 million in 2040 (Wilson et al. 2019), and a similar rise is expected for Alzheimer's and Parkinson's disease (Reeve et al. 2014). Compression of late-life morbidity is, therefore, a priority to alleviate suffering in the elderly (Partridge et al. 2018) and to reduce a growing economic burden to society (Rae et al. 2010).

Critically, seminal discoveries in the biology of ageing showed that ageing is a malleable process and that down-regulation of major cellular nutrient signalling pathways, either glucose-sensing insulin signalling or amino acid-sensing target-of-rapamycin signalling, results in longevity and health improvement in all model organisms tested from yeast to mammals (Lopez-Otin et al. 2013). For instance, the long-lived mutants in *C. elegans* are protected from tumorous cell proliferation (Pinkston et al. 2006) and have reduced toxic protein aggregation (Cohen et al. 2006), while *Drosophila* show less deterioration in their hearts (Wessells et al. 2004). Long-lived mouse mutants are protected from osteoporosis, cataracts and skin pathology, as well as decline in glucose homeostasis, immune and motor function (Selman et al. 2008). The effect of these mutations is conserved from yeast to mammals, and it is, therefore, expected that if drugs replicate the biological impact of these changes, this could improve health in the elderly and prevent age-related disease. It is increasingly recognised that directly targeting ageing through pharmacological interventions, as opposed to specific age-related diseases, is a highly promising strategy for broad-spectrum disease protection (Niccoli and Partridge 2012). However, at present, there are only a handful of reliable anti-ageing drugs whose effects have been confirmed in mammals, such as rapamycin (Harrison et al. 2009) and metformin (Martin-Montalvo et al. 2013). Crucially, there are currently no sufficiently reliable ageing biomarkers for testing drugs on human cells *in vitro,* and the development of a specialised epigenetic clock is a promising approach (Castillo-Quan et al. 2015; Field et al. 2018; Horvath et al. 2018; Bell et al. 2019; Horvath et al. 2019).

To accelerate the discovery workflow for anti-ageing drugs, we took advantage of the breakthrough in the ageing field which showed that epigenetic clocks provide the most accurate measurements of human age. For instance, the approximate error rate for the Skin and Blood clock is ±2.5 years (maximal correlation coefficient 0,98) (Horvath et al. 2018). Epigenetic clocks surpass the accuracy of other ageing biomarkers such as telomere length and those based on transcriptomic, metabolomic or proteomic approaches, potentially because the latter approaches detect more transient and less stable cellular changes (Horvath 2013). Ageing is accompanied by overall CpG hypomethylation, whilst some CpG islands and gene regions become hypermethylated (Booth and Brunet 2016). Remarkably, only a small selection of the 56 million CpG sites in the diploid human

genome, coupled with computational algorithms, is sufficient to provide an accurate readout of human age. One of the first epigenetic clocks was developed by Hannum using just 71 CpG sites to estimate age from blood samples (Hannum et al. 2013), while Horvath's multi-tissue age estimator (Horvath 2013) and Skin and Blood clock (Horvath et al. 2018) use 353 and 391 CpG sites, respectively (Field et al. 2018; Horvath and Raj 2018). Even a single CpG site in the ELOVL2 gene is sufficient to determine age (Garagnani et al. 2012), albeit clocks using only a few CpG sites are less accurate and less applicable to different tissues (Horvath and Raj 2018). The epigenetic clocks measure the ageing process inherent to all our cells and tissues, irrespective of their proliferation rate (Horvath et al. 2019). As the human epigenome reflects physiological changes, epigenetic clocks cannot only predict chronological age from a human sample but also give an estimate of biological age as has widely been demonstrated by the associations of epigenetic age with morbidity and mortality (Marioni et al. 2015; Horvath and Raj 2018). Recently, valuable predictors focussing on this aspect have been developed: PhenoAge (Levine et al. 2018) and GrimAge (Lu et al. 2019), which form the best epigenetic morbidity and mortality predictors available to date.

DNA methylation also captures information on the approximate number of cell divisions a cell has been through, as has been shown by epiTOC (Yang et al. 2016), a mitotic-like clock that approximates stem cell divisions and correlates with cancer risk (Tomasetti et al. 2017), and MiAge, which also measures mitotic age (Youn and Wang 2018). The biology underlying CpG methylation alterations at the sites linked to ageing clocks is not well understood. The exception is ribosomal clock based on CpG methylation in ribosomal RNA (rRNA), which is highly conserved throughout evolution and which forms nucleolus that has itself been implicated in ageing (Tiku and Antebi 2018; Wang and Lemos 2019). Horvath suggests an interesting hypothesis that epigenetic maintenance programmes are being reflected in DNA methylation alterations (Horvath 2013; Horvath and Raj 2018; Raj and Horvath 2020). Recent findings implicate loss of H3K36 histone methyltransferase NSD1 in epigenetic ageing clock acceleration (Martin-Herranz et al. 2019). Despite the enigma regarding the mechanism of epigenetic clocks, they are reliable predictors of age and extremely useful biomarkers (Field et al. 2018; Horvath and Raj 2018; Bell et al. 2019). However, little is known so far about the performance of these clocks in *in vitro* ageing experiments. It has recently been shown that the rate of epigenetic ageing in cultured cells is significantly faster than in the human body (Horvath et al. 2019; Sturm et al. 2019) and that epigenetic age is retarded by rapamycin *in vitro* (Horvath et al. 2019), but neither of the clocks specialised for *in vitro* drug discovery nor were they tested on multiple anti-ageing drugs.

Therefore, we aimed to exploit the exceptional accuracy of CpG methylation clocks to uncover new anti-ageing pharmacological treatments. The current gold standard for discovering novel anti-ageing drugs are longevity experiments, which are laborious, lengthy and expensive. For instance, in mice, they take three years, thereby precluding any large scale drug screens. Existing screens in *C. elegans* commonly use live *E. coli* as food (Lucanic et al. 2013; Ye et al. 2014), which is a

120 disadvantage as drugs are metabolised first by the bacteria making their effect on worms secondary,
121 which may lead to confounded results (Cabreiro et al. 2013; Pryor et al. 2019). Yeast drug screens
122 lack the crucial aspect of tissue toxicity (Zimmermann et al. 2018). In addition, all longevity assays
123 require constant supply of the drug, making them highly expensive. Other attempts to uncover anti-
124 ageing effects of drugs are based on computational analysis using existing transcriptomic
125 information on the ageing process combined with drug characteristics (Donertas et al. 2018).
126 However, transcriptomic changes are more transient and noisy when compared to DNA methylation
127 and are, therefore, a less consistent ageing marker (Horvath and Raj 2018).

128 We tested if existing epigenetic clocks could be used to measure anti-ageing drug potential in human
129 primary cells *in vitro* and if we could build a new clock specialised for this purpose. Senescence is
130 tightly associated with ageing of the organism, and because of the pronounced resemblance of
131 ageing in primary cells *in vitro* to ageing *in vivo,* together with the evidence that human DNA
132 methylation signatures are conserved and accelerated in cultured fibroblasts (Sturm et al. 2019), we
133 used cultured human cells as a proxy for human ageing (Lowe et al. 2015; Horvath et al. 2019). The
134 ability to test anti-ageing drug properties directly on human cells *in vitro* could considerably
135 accelerate the discovery of new compounds promoting healthy ageing. To this end, we used normal
136 human mammary fibroblasts (HMFs) from a healthy 16-year old donor that we cultured from
137 passage 10 to passage 20, which is before these cells reach senescence at passage 29
138 (Supplemental Fig. S1A-D). To measure CpG methylation, we used EPIC Arrays (Illumina) that
139 measure methylation at 850,000 sites.

140 First, we tested the three most suitable existing epigenetic clocks, to determine if they could detect
141 weekly and monthly ageing differences occurring during serial passaging of HMFs (Fig. 1A). The
142 Multi-tissue clock (Horvath 2013) consistently predicted a higher epigenetic age, and at passage ten
143 this was 43.6±1.0 years (Fig. 1A), consistent with what was recently reported (Sturm et al. 2019).
144 This increased age estimate, compared to the age of the donor who was 16 years old, is in
145 accordance with published data demonstrating that this epigenetic clock overestimates the age of
146 mammary tissue samples (Horvath 2013). The PhenoAge clock (Levine et al. 2018), developed to
147 predict mortality and morbidity risks, reported the epigenetic age of the donor to be 3.5±1.1 years
148 (Fig. 1A). The most accurate age estimate, predicting the age of the donor at 23.2±0.87 years, was
149 obtained using the Skin and Blood clock, which is specialised for determining donor age of easily
150 accessible human tissues and cells in culture (Fig. 1A). The Multi-tissue clock and Skin and Blood
151 clock showed a small increase in age with progressive passaging (from passage 10 to 20, age
152 estimate increased from 43.6±1.0 to 53.9±1.7 and from 23.2±0.87 to 31.6±1.2 years, respectively),
153 while this increase was greater for the PhenoAge clock (from 3.5±1.1 to 26.6±9.7 years). This
154 suggested that, of the tested clocks, the PhenoAge clock captures ageing *in vitro* best (Fig. 1A).
155 However, the PhenoAge clock showed substantial variability in predictions for higher passages,
156 which would obstruct the detection of subtle ageing differences upon anti-ageing drug treatments. In

conclusion, while the Skin and Blood clock (Horvath et al. 2018) measures fibroblast ageing in culture, none of the existing clocks was ideally suited to accurately measure subtle anti-ageing drug potential in human primary cells *in vitro,* and similar comparisons have recently been reported by others (Horvath et al. 2019; Sturm et al. 2019).

This prompted us to develop a new clock that, rather than predicting donor age in years, specialises in measuring methylation changes occurring during ageing of primary cells in culture and could differentiate DNA methylation state between each passage. To this end, we developed a clock using two different cell types, the above-mentioned HMFs and human dermal fibroblasts (HDFs), which were obtained from a different donor, have a different proliferative lifespan *in vitro*, and a different rate of DNA methylation change. Like the HMFs, the HDFs were serially passaged and sampled every other passage for DNA methylation analysis.

We used a total of 39 HMF and HDF samples to build the clock (see Materials and methods). To preselect informative probes, we performed a statistical test to identify CpGs undergoing DNA methylation changes with increasing cell passage using linear regression (Supplemental Fig. S2A). The resulting 2,543 CpGs were used to build the clock model by elastic net regression, similar to the method used by Horvath (Horvath 2013). The model selected 42 predictor CpGs ("clock CpGs"), shown in Fig. 1B and Supplemental Fig. S2B. Of these CpGs, 23 undergo hypomethylation and 19 become hypermethylated with increasing cell passage (Fig. 1B and Supplemental Fig. S2B). Sixteen of the CpGs are located in intergenic regions (IGRs), whereas 14 of them are located in gene bodies and 12 in promoters, respectively (Supplemental Fig. S2C). Interestingly, two of the clock CpGs map to gene *GRID1,* one is located in its 3'UTR and one in the gene's body. *GRID1* encodes a subunit of glutamate receptor channels. Several other clock CpGs are also located in genes implicated in cell receptor activity and metabolic processes, such as *LDLRAD4 and NPSR1*. Furthermore, multiple clock CpGs map to genes that play roles development as well as in the regulation of transcription and protein binding. Examples include *GGN, MEIS2, NF1, PROP1, RFX4, RUNX3* and *SMARCA2*. The 42 CpGs together with their detailed genomic and functional annotation are available in Table 1.

After building our novel epigenetic clock to measure cell ageing *in vitro*, named CellAgeClock, we tested its performance using an entirely different set of samples (n=26), consisting of 22 HMF and four HDF samples. We observed accurate prediction of passage number for both HMFs and HDFs, with a Root Mean Square Error (RMSE) of 0.37 (Fig. 1C). To compare the performance of the CellAgeClock with other epigenetic age predictors, we calculated Spearman's rank correlation coefficients between the clocks' output and actual cell passage (see Table 2). The CellAgeClock showed the best correlation among the tested predictors, with Spearman's Rho$=0.98$ and $p<2.2e-16$. We also tested the mitotic-like clocks EpiTOC and MiAge, for comparison. However, their correlation coefficients were negative, small and non-significant (Rho>-0.3, $p>0.05$).

193 Having built a precise epigenetic clock that measures methylation changes during replicative ageing
194 of human primary cells *in vitro*, we tested if anti-ageing drug treatment of HMFs and HDFs
195 decelerated the CellAgeClock. We chose an mTOR inhibitor, rapamycin, which is one of the most
196 robust and evolutionarily conserved anti-ageing drug targets (Saxton and Sabatini 2017), and which
197 mediates its effect through down-regulation of S6K and Pol III, and up-regulation of autophagy
198 (Bjedov et al. 2010; Filer et al. 2017). We chose relatively low rapamycin concentration of 5nM that
199 did not inhibit cell growth (Supplemental Fig. S1A) but moderately downregulated mTOR signalling,
200 as evidenced by decreased pS6K and p4E-BP phosphorylation (Supplemental Fig. S3). This setup
201 mimics the pro-longevity effects of rapamycin *in vivo* where it is well accepted that only mild nutrient
202 sensing pathway inhibition increases life- and healthspan (Bjedov and Partridge 2011; Lopez-Otin et
203 al. 2013).

204 DNA methylation profiles from HDF and HMFs collected following four, six and eight weeks of
205 rapamycin treatment (passage 16, 18 and 20; Fig. 2) were analysed using the CellAgeClock and
206 clearly demonstrated that rapamycin slows down methylation changes associated with replicative
207 ageing. Interestingly, this clock deceleration was more pronounced upon longer treatment as shown
208 by the gradual decrease of predicted-actual passage from 16 to 20 weeks. The low dose rapamycin
209 treatment did not affect population doublings, confirming that the methylation changes were not a
210 reflection of proliferation inhibition or slowing of the cell cycle (Supplemental Fig. S1). This is further
211 evidenced by comparing the predicted passage from the CellAgeClock against cumulative
212 population doubling, showing that rapamycin samples lie on a separate line to that of the control
213 samples (Supplemental Fig. S4A-B). Contrarily, rapamycin samples and controls differed to
214 considerably lesser extent when actual passage and cumulative population doublings are compared
215 (Supplemental Fig. S4A-B). We observed a similar pattern for HMFs and HDFs (Fig. 2), suggesting
216 that the CellAgeClock is applicable to different cells, albeit calibration is required for cells that reach
217 senescence at different rates.

218 We then focused on HMFs to test another anti-ageing drug, trametinib (Slack et al. 2015), an
219 inhibitor of the MEK/ERK signalling pathway, which we also applied in low concentration to avoid
220 any effect on growth and population doubling (Supplemental Fig. S1B and S3). The CellAgeClock
221 analysis of trametinib treatment showed clock deceleration for all three passages tested (Fig. 2),
222 thereby confirming previous results in *Drosophila in vivo* that trametinib extends lifespan (Slack et al.
223 2015). Next, we examined the effect of two other inhibitors of nutrient-sensing pathways as
224 mutations in these pathways in model organisms represent the most evolutionary conserved anti-
225 ageing interventions (Lopez-Otin et al. 2013). We tested Dactolisib/BEZ235, a dual ATP competitive
226 PI3K and mTOR inhibitor, for which we again optimised the dose of the treatment to obtain a
227 reduction in signalling, as shown by pS6K downstream target 4E-BP (Supplemental Fig. S3), without
228 significant proliferation impairment (Supplemental Fig. S1C). Dactolisib/BEZ235 slowed down the
229 DNA methylation changes similar to rapamycin, suggesting that Dactolisib/BEZ235 could be a new

230 anti-ageing drug according to the output of the CellAgeClock (Fig. 2). We also tested torin2, which is
231 a selective inhibitor of the mTOR pathway that inhibits both mTORC1 and mTORC2, unlike
232 rapamycin, which targets solely mTORC1. Owing to its more complete inhibition of the mTOR
233 pathway, we were interested in examining its effect on replicative ageing, especially as the role of
234 mTORC2 in ageing is less well established. The impact of mTORC2 inhibition on lifespan can be
235 positive or negative depending on which of the mTORC2 downstream effectors is affected, in which
236 tissue, and whether females or male mice are used for the experiment (Kennedy and Lamming
237 2016). Some of the negative effects of mTOR pathway inhibition, such as insulin resistance and
238 hyperlipidemia, are attributed to the mTORC2 branch of the pathway and may arise under certain
239 conditions of prolonged and/or high dose rapamycin treatment (Kennedy and Lamming 2016).
240 Interestingly, while our CellAgeClock suggests that torin2 is indeed a novel anti-ageing drug (Fig. 2,
241 Supplemental Fig. S1D and S3), its effect on ageing in mammalian cell culture appears to be less
242 pronounced than that of rapamycin. This is in line with literature suggesting that a promising strategy
243 to improve healthy ageing is the development of inhibitors that are highly specific for mTORC1 or
244 that target mTORC1 downstream effectors separately (Kennedy and Lamming 2016).

245 Next, we compared our anti-ageing drug screening results obtained by the CellAgeClock with
246 analyses using Horvath's Multi-tissue and Skin and Blood clock, as well as the PhenoAge clock. The
247 clocks did not detect any significant effect of anti-ageing drug treatment (Supplemental Fig. S5). The
248 Skin and Blood clock[26] was used recently to measure deceleration of ageing in primary fibroblasts
249 (Horvath et al. 2019; Sturm et al. 2019), however the concentration of rapamycin used in our
250 conditions was five times lower without effect on cell growth, highlighting the sensitivity of our
251 epigenetic clock to detect age-related methylation changes at very low drug concentrations. Under
252 our conditions, the only epigenetic clock that detected gradual methylation changes from passage 10
253 to passage 20 was the PhenoAge clock (Supplemental Fig. S5). However, its output was more
254 variable between samples and inconsistent for anti-ageing drug treatments, reporting both clock
255 acceleration and deceleration. For instance, rapamycin, Dactolisib/BEZ235 and torin2 treated cells
256 appeared slightly younger compared to controls, whereas trametinib treated cells were estimated
257 older to some extent (Supplemental Fig. S5), unlike the results we obtained with our CellAgeClock
258 (Fig. 2). Overall, the CellAgeClock that we developed here was more consistent and performed
259 significantly better on ageing cells in culture and following known anti-ageing drug treatments
260 compared to existing clocks. Our results are supportive of clocks being highly specialised for a
261 certain task, and suggests that while other popular epigenetic clocks perform remarkably on
262 determining donor's age in years and their health status, they were not able to robustly detect slight
263 ageing changes in human primary cells induced by drug treatment over a short period of time *in*
264 *vitro*.

265 Next, we assessed if the CellAgeClock is suitable for the screening of novel anti-ageing drugs. To
266 this aim, we examined if drugs that decelerate the CellAgeClock also reduce features associated

267 with senescence, such as morphological changes and expression of ageing biomarkers
268 (Hanzelmann et al. 2015). Rapamycin, Dactolisib/BEZ235 and Trametinib treatment slowed down
269 morphological alteration in cells that gradually occur during replicative ageing, namely cell
270 elongation, increased nuclear area and cell area, and the treated cells appeared particularly
271 'youthful' (Fig. 3). Another characteristic of senescence is increased expression of the cyclin-
272 dependent kinase inhibitors $p21^{CIP1/Waf1}$ and $p16^{INK4a}$. $p21^{CIP1/Waf1}$ triggers G1 cycle arrest upon
273 damage and can lead to senescence or apoptosis (He and Sharpless 2017; McHugh and Gil 2018).
274 Expression of $p16^{INK4a}$, which is produced from the CDKN2A gene together with $p19^{ARF}$ ($p14^{ARF}$ in
275 humans) increases exponentially during ageing and was suggested to stabilise the senescent state
276 (Gire and Dulic 2015). $p16^{INK4a}$ expression was the marker of choice for senescent cell clearance
277 leading to prolonged lifespan in mice (Baker et al. 2016).

278 Our results demonstrate that drugs which decelerate the CellAgeClock at the same time reduce
279 expression of both nuclear $p21^{CIP1/Waf1}$ and $p16^{INK4a}$ compared to non-treated cells, showing their
280 efficacy in delaying the senescence programme (Fig. 3B-C). In addition, the most frequently used
281 senescent marker, senescent-associated β-galactosidase activity (SA-βgal), was significantly
282 decreased upon anti-ageing drugs treatment with rapamycin and Dactolisib/BEZ235, but not in cells
283 treated with trametinib (Fig. 3B-C). Another difference in senescent markers was observed with
284 interleukin-6 (IL-6), which is one of the most important inflammatory cytokines and part of the
285 senescent-associated secretory phenotype. IL-6 was significantly reduced in aged cells upon
286 rapamycin and Dactolisib/BEZ235 treatment but not in trametinib treated cells (Fig. 3B-C). This
287 difference possibly stems from the overactivated RAS/ERK pathway being a more prominent inducer
288 of senescence than the overactivated mTOR/PI3K pathway (Kennedy et al. 2011), and hence
289 corresponding inhibitors have different potency in inhibiting senescence. Finally, we examined the
290 nucleolus, an organelle dedicated to rRNA production and ribosomal assembly, as it has recently
291 emerged that maintenance of its structure, and low levels of nucleolar methyltransferase fibrillarin, is
292 a common denominator for major anti-ageing intervention from worms to mice (Tiku and Antebi
293 2018). We observed that as a consequence of ageing, nucleoli in aged HMFs lose their defined
294 round shape, are more diffused, and stain less well. For rapamycin and Dactolisib/BEZ235, we
295 observed clearly defined and 'younger' looking nucleoli in aged cells. However, trametinib treated
296 cells resembled the nucleoli of controls. In summary, a panel of the most frequently used markers for
297 cell senescence confirmed that drugs which decelerate the CellAgeClock also make the cells appear
298 more youthful. This strongly suggests that the CellAgeClock can be used as a robust and sensitive
299 detector of novel anti-ageing treatments.

300 Finally, having discovered two novel potential anti-ageing drug treatments using the CellAgeClock,
301 Dactolisib/BEZ235 and torin2, we tested and validated them *in vivo* using the fruit fly *Drosophila*
302 *melanogaster* as a model organism. This is important as tissue-specific drug toxicity, which can be
303 missed in cell culture, is one of the major reasons for drug failure in clinical trials. For *in vivo*

longevity studies we used the outbred wild-type w^{Dah} strain which is particularly suitable for ageing studies, Drosoflipper device for fast fly transfer, and specially formulated holidic medium (Piper et al. 2014) to increase drug bioavailability compared to standard sugar-yeast-agar fly food. We used rapamycin as a positive control for longevity experiments in flies and showed that median lifespan extension on holidic media varied from 7% to 9% compared to ethanol solvent control, depending on 1μM or 5μM concentration, respectively ($p<0.001$, log-rank test), which is comparable to published literature (Fan et al. 2015) (Fig. 4A). Importantly, both Dactolisib/BEZ235 and torin2 significantly extended lifespan in *Drosophila* for 7% ($p<0.001$, log-rank test) (Fig. 4B-C). This firmly demonstrates that drugs that decelerate the CellAgeClock have similarly favourable output on major anti-ageing biomarkers *in vitro* and extend longevity *in vivo* (Fig. 4D).

For the first time, we have a robust epigenetic clock for the rapid discovery of anti-ageing drugs directly in human cells, bypassing lower model organisms and significantly shortening discovery time compared to 3-year long mice longevity analysis. Testing different compounds for ageing using the CellAgeClock could potentially reveal new anti-ageing pathways and help us to improve our knowledge base of not only ageing biology but of molecular pathways underpinning the epigenetic clocks as well, understanding of which is limited. Other available epigenetic clocks could not accurately detect the effect of low-dose short-term anti-ageing drugs on cells *in vitro*. We expect many biological outputs to be extracted by the CellAgeClock and other epigenetic clock algorithms in the future, given the wealth of information stored in our epigenome.

Better experimental systems to test anti-ageing drugs are very much needed, given a rising proportion of the elderly in modern societies and, as a consequence, larger numbers of people suffering from age-related diseases. Our results show that by using the CellAgeClock, cultured primary human cells can be used as a proxy to measure human ageing and can reliably detect anti-ageing effects upon a relatively brief treatment. By doing so, this fast and accurate method is expected to accelerate the discovery of novel preventive treatments for age-related disease, directly using human cells. Importantly, follow-up research will be focused on expanding our findings on different types of primary cells from donors of different ages, as well as on testing further compounds. While ageing itself is not a disease, potential anti-ageing drugs could be FDA approved separately for different conditions. The first study to test broad-spectrum protection capacity of metformin, the TAME study, is underway (Barzilai et al. 2016). In addition, it was shown that rapamycin/everolimus pre-treatment dramatically improves flu vaccination and immune response in the elderly (Mannick et al. 2018). In mice, it also lowers the incidence of tumours (Anisimov et al. 2011), and it shows promising results in the field of neurodegeneration (Bove et al. 2011). This supports the idea that targeting healthy ageing might have multiple beneficial outputs.

Our novel drug discovery platform will inform on new anti-ageing mechanisms, currently dominated by IIS and mTOR signalling pathways as well as dietary restriction regimes. Many drugs targeting

342 growth pathways are already available from cancer research where they are used in very high
343 doses. With the CellAgeClock, we examined which of these compounds could be disease
344 preventative at very low concentrations. Our experimental setup is also suitable for nutraceutical
345 approaches whereby dietary supplements can be rigorously tested for their effect on ageing. Overall,
346 we expect our novel discovery platform to accelerate the discovery of strongly sought after anti-
347 ageing drugs and geroprotective strategies to improve healthy human ageing.
348
349 **Materials and methods**
350 **Cell culture and reagents.** Normal finite lifespan human mammary fibroblasts (HMFs) were
351 obtained from reduction mammoplasty tissue of a 16-year-old individual, donor 48 by Dr Martha
352 Stampfer (University Berkeley) who has all required IRB approvals to distribute these cell samples
353 and MTA agreement set in place with Dr Cleo Bishop laboratory. Independent cultures from these
354 cells were serially passaged from passage 9 through to passage 20 and aliquots taken upon each
355 passage for Illumina Infinium Methylation EPIC analysis. HMFs were maintained in Dulbecco's
356 Modified Eagles Medium (DMEM) (Life Technologies, UK) supplemented with 10% foetal bovine
357 serum (FBS) (Labtech.com, UK), 2mM L-glutamine (Life Technologies, UK) and 10 µg/mL insulin
358 from bovine pancreas (Sigma).
359 Normal finite lifespan human dermal fibroblasts (HDFs) were obtained from face lift dermis following
360 a kind donation from an anonymous healthy patient under standard ethical practice, reference LREC
361 No. 09/HO704/69. HDFs were grown in DMEM with 4 mM L-glutamine (Life Technologies),
362 supplemented with 10% FBS.
363 Cells were plated at 7,500 cells/cm^2 in T25 cell culture flask in 5ml of media to which 5µl of
364 appropriate drug or vehicle control was added. Media was changed every two days and cells were
365 passaged every 7 days and trypsinisation was used to detach the cells. All cells were routinely
366 tested for mycoplasma and shown to be negative.
367
368 **Immunofluorescence microscopy and high content analysis.** Cells were washed in phosphate
369 buffered saline (PBS), fixed for 15 minutes with 3.7% paraformaldehyde with 5% sucrose, washed
370 and permeabilised for 15 minutes using 0.1% Triton X in PBS (30 minutes for anti-nucleolin
371 antibody) then washed and blocked in 0.25% bovine serum albumin (BSA) in PBS before primary
372 antibody incubations. Primary antibodies used were anti-IL6 (R&D Systems, 1:100; overnight 4°C),
373 anti-nucleolin (Santa Cruz, 1:2000, overnight room temperature), anti-p16 (Proteintech, 1:500,
374 overnight 4°C), anti-p21 (12D1, Cell Signalling, 1:2000, overnight 4°C). Cells were incubated for 2
375 hours at room temperature with the appropriate AlexaFluor-488, AlexaFluor-546 or AlexaFluor-647
376 conjugated antibody (1:500, Invitrogen), DAPI (1:1,000 from 1mg/mL stock) and CellMask Orange or
377 Deep Red (1:200,000, Invitrogen). Images were acquired using the IN Cell 2200 or 6000 automated
378 microscope (GE) and HCA was performed using the IN Cell Developer software (GE).
379

380 **Z score generation.** For each of the parameters analysed, significance was defined as one Z score
381 from the negative control mean. Z scores were generated according to the formula below: Z score =
382 (mean value of experimental condition – mean value of vehicle control/standard deviation (SD) for
383 vehicle control.
384
385 **Senescence-associated beta-galactosidase (SA-β-Gal) assay.** Cells were washed in PBS, fixed
386 for 5 minutes with 0.2% glutaraldehyde, washed and incubated for 24 hour at 37°C (no CO_2) with
387 fresh senescence-associated beta-galactosidase (SA-β-Gal) solution: 1mg of 5-bromo-4-chloro-3-
388 indoyl β-D-galactosidase (X-Gal) per mL (stock = 20mg of dimethylsulfoxide per ml) / 40mM citric
389 acid/sodium phosphate, pH 6.0 / 5mM potassium ferrocyanide / 5mM potassium ferricyanide /
390 150mM NaCl / 2mM $MgCl_2$). Cells were stained with Hoechst 33342 (1:10,000 from 10mg/mL stock)
391 for 30 minutes. Images were acquired using the IN Cell 2200 automated microscope and HCA was
392 performed using the IN Cell Developer software.
393
394 **Genomic DNA extraction.** For isolation of Genomic DNA from primary human fibroblasts we used
395 QIAamp DNA micro kit (56304) and we followed manufacturers protocol, with an additional washing
396 steps with 500μl AW2 buffer and 500μl 80% ethanol to improve purity. DNA quantification and purity
397 was determined by Nanodrop and QuBit. For bisulfite conversion EZ DNA methylation kit was used
398 (D5001).
399
400 **Preparation of methylation array data.** For each sample, 500ng high-quality DNA was bisulphite
401 converted using the EZ DNA methylation kit (Zymo Research), using the alternative incubation
402 conditions recommended for use with Illumina methylation arrays. Bisulphite converted DNA was
403 eluted in 12ul elution buffer. Methylation was analysed using the Infinium Human Methylation EPIC
404 array (Illumina) using standard operating procedures at the UCL Genomics facility. The EPIC array
405 data have been deposited into ArrayExpress at the European Bioinformatics Institute
406 (https://www.ebi.ac.uk/arrayexpress/) under accession number E-MTAB-8327.
407
408
409 **Pre-processing of methylation array data.** DNA methylation array data was processed using the
410 minfi package (Fortin et al. 2017) within R (R Core Team, 2013). Initial QC metrics from this package
411 were used to remove low-quality samples. Probes were filtered using a detection p-value cut-off
412 >0.01 and normalised using the Noob procedure. Cross-hybridising probes were removed from
413 analysis based on the list published in McCartney et al. (McCartney et al. 2016). The training and
414 test sets were pre-processed separately to obtain a fair estimate of the performance of the
415 CellAgeClock.
416
417 **Estimation of sample age using existing epigenetic clocks.** Following pre-processing of data,
418 the epigenetic age of all samples was predicted using three epigenetic clocks; the Multi-tissue clock

419 (Horvath 2013), the Skin and Blood clock (Horvath et al. 2018) and the PhenoAge clock (Levine et
420 al. 2018) using the online DNA methylation calculator at http://dnamage.genetics.ucla.edu (Horvath
421 2013).
422
423 **Development of the CellAgeClock.** The clock was built using a total of 39 samples, with six
424 samples at each of the following passages; 10, 12, and 14; and seven samples at each of the
425 following passages; 16, 18, and 20. This included both HDFs (n=12) and HMFs (n=27). 730,453
426 probes passed quality control measurements as described in the pre-processing section. A
427 differential DNA methylation test was performed on this set of probes to identify CpGs undergoing
428 significant DNA methylation changes with increasing cell passage. We used the linear regression
429 approach for continuous variables implemented in minfi's DMPFinder function (Fortin et al. 2017).
430 This resulted in 2,543 differentially methylated CpGs at a p-value threshold of $1x10^{-11}$ which was
431 selected using leave one out validation. Next, we built the clock model by elastic net regression
432 using the DNA methylation levels of the 2,543 CpGs across all passages as input. We applied the
433 glmnet function of the corresponding R package (Friedman et al. 2010) setting alpha to 0.5 and
434 determining the lambda parameter by the internal cross validation function provided by glmnet. The
435 elastic net regression model selected 42 CpGs as predictors of cell passage (Supplemental Table 1).
436 We obtained the genomic annotation of these CpGs from Illumina's EPIC manifest, and retrieved
437 gene functions using DAVID (Huang da et al. 2009) where we selected the following sources for
438 annotation: GOTERM_BP_DIRECT, GOTERM_CC_DIRECT, GOTERM_MF_DIRECT,
439 ENTREZ_GENE_SUMMARY, OFFICIAL_GENE_SYMBOL and KEGG_PATHWAY.
440 We then tested the CellAgeClock on a different set of 26 samples, 22 HMFs and 4 HDFs, across the
441 following passages: 9 (1 HMFs), 10 (2 HMFs), 11 (2 HMFs), 12 (1 HMFs), 13 (2 HMFs), 14
442 (2 HMFs), 15 (2 HMFs), 16 (4 HMFs and 2 HDFs), 18 (3 HMFs and 1 HDFs) and 20 (3 HMFs and
443 1 HDFs).
444
445 **Availability of the CellAgeClock.** The CellAgeClock is available as a Jupyter Notebook in Python
446 and can be retrieved from https://github.com/ucl-medical-genomics/CellAge-epigenetic-clock.
447
448 **Lifespan measurements.** We used *white Dahomey* (w^{Dah}) wild-type flies that were maintained and
449 all experiments were conducted at 25ºC. Flies were kept on a 12 h light:12 h dark cycle at constant
450 humidity using standard sugar/yeast/agar (SYA) medium. For all experiments, flies were reared at
451 standard larval density by transferring 18 μl of egg suspension into SYA bottles. Eclosing adults
452 were collected over a 12-h period and allowed to mate for 48 h before sorting into single sexes and
453 placed in vials containing either control or experimental drug food. For lifespan assays, flies were
454 reared at standard density and maintained at 15 flies per vial and we used holidic media recipe food
455 for all longevity assays (Piper et al. 2014). Flies were transferred to fresh food vials every 2-3 days
456 and scored for deaths. At least 150 flies were used for each lifespan experiment.
457

Western blot measurements. Whole flies or human primary cell pellet was homogenised in 2x Laemmli loading sample buffer (100 mM Tris pH 6.8, 20% glycerol, 4% SDS; Bio-Rad) containing 50 mM DTT, protease inhibitor (cOmplete Mini EDTA-free; Roche) and phosphatase inhibitor (PhosSTOP EASYpack; Roche) cocktails. Extracts were cleared by centrifugation and approximately 20 µg of protein extract was loaded per lane on a polyacrylamide gel. Proteins were separated and transferred to nitrocellulose membrane. The following antibodies were used at the indicated dilutions: H3 (Cell Signaling Technology; 1:2000; 4499S), pS6K (Cell Signaling Technology; 1:1000; 9206S), total S6K (Santa Cruz; 1:1000; 8418), p4EBP (Cell Signalling Technology, 1:500; 2855S), non-phospho4E-BP (Cell Signalling Technology; 1:500; 4923S), pAkt (Cell Signalling; 1:1000; 4060), pAkt (Cell Signalling; 1:1000; 4056), total Akt (Cell Signalling; 1:1000; 9272), pERK (Cell Signalling; 1:1000; 4370), total (Cell Signalling; 1:1000; 4692). Blots were developed using the ECL detection system (GE, Amersham), and analysed using FIJI software (US National Institutes of Health). We used precasted TGX stain-free gels from Bio-Rad (567-8123 or 567-8124) according to the manufacturer's instructions.

Statistical analysis. Statistical analysis was performed using R. Log-rank tests were performed on lifespan curves.

Online content

The CellAgeClock is available from GitHub at https://github.com/ucl-medical-genomics/CellAge-epigenetic-clock. All methylation microarray data reported in this study have been deposited in the ArrayExpress (https://www.ebi.ac.uk/arrayexpress/) public repository and are accessible under accession number E-MTAB-8327.

References

Anisimov VN, Zabezhinski MA, Popovich IG, Piskunova TS, Semenchenko AV, Tyndyk ML, Yurova MN, Rosenfeld SV, Blagosklonny MV. 2011. Rapamycin increases lifespan and inhibits spontaneous tumorigenesis in inbred female mice. *Cell Cycle* **10**: 4230-4236.

Baker DJ, Childs BG, Durik M, Wijers ME, Sieben CJ, Zhong J, Saltness RA, Jeganathan KB, Verzosa GC, Pezeshki A et al. 2016. Naturally occurring p16(Ink4a)-positive cells shorten healthy lifespan. *Nature* **530**: 184-189.

Barzilai N, Crandall JP, Kritchevsky SB, Espeland MA. 2016. Metformin as a Tool to Target Aging. *Cell Metab* **23**: 1060-1065.

Bell CG, Lowe R, Adams PD, Baccarelli AA, Beck S, Bell JT, Christensen BC, Gladyshev VN, Heijmans BT, Horvath S et al. 2019. DNA methylation aging clocks: challenges and recommendations. *Genome Biol* **20**: 249.

Bjedov I, Partridge L. 2011. A longer and healthier life with TOR down-regulation: genetics and drugs. *Biochem Soc Trans* **39**: 460-465.

497 Bjedov I, Toivonen JM, Kerr F, Slack C, Jacobson J, Foley A, Partridge L. 2010. Mechanisms
498 of life span extension by rapamycin in the fruit fly Drosophila melanogaster. *Cell*
499 *Metab* **11**: 35-46.
500 Booth LN, Brunet A. 2016. The Aging Epigenome. *Mol Cell* **62**: 728-744.
501 Bove J, Martinez-Vicente M, Vila M. 2011. Fighting neurodegeneration with rapamycin:
502 mechanistic insights. *Nat Rev Neurosci* **12**: 437-452.
503 Cabreiro F, Au C, Leung KY, Vergara-Irigaray N, Cocheme HM, Noori T, Weinkove D,
504 Schuster E, Greene ND, Gems D. 2013. Metformin retards aging in C. elegans by
505 altering microbial folate and methionine metabolism. *Cell* **153**: 228-239.
506 Castillo-Quan JI, Kinghorn KJ, Bjedov I. 2015. Genetics and pharmacology of longevity: the
507 road to therapeutics for healthy aging. *Adv Genet* **90**: 1-101.
508 Cohen E, Bieschke J, Perciavalle RM, Kelly JW, Dillin A. 2006. Opposing activities protect
509 against age-onset proteotoxicity. *Science* **313**: 1604-1610.
510 Donertas HM, Fuentealba Valenzuela M, Partridge L, Thornton JM. 2018. Gene expression-
511 based drug repurposing to target aging. *Aging Cell* **17**: e12819.
512 Fan X, Liang Q, Lian T, Wu Q, Gaur U, Li D, Yang D, Mao X, Jin Z, Li Y et al. 2015. Rapamycin
513 preserves gut homeostasis during Drosophila aging. *Oncotarget* **6**: 35274-35283.
514 Field AE, Robertson NA, Wang T, Havas A, Ideker T, Adams PD. 2018. DNA Methylation
515 Clocks in Aging: Categories, Causes, and Consequences. *Mol Cell* **71**: 882-895.
516 Filer D, Thompson MA, Takhaveev V, Dobson AJ, Kotronaki I, Green JWM, Heinemann M,
517 Tullet JMA, Alic N. 2017. RNA polymerase III limits longevity downstream of TORC1.
518 *Nature* **552**: 263-267.
519 Fortin JP, Triche TJ, Jr., Hansen KD. 2017. Preprocessing, normalization and integration of
520 the Illumina HumanMethylationEPIC array with minfi. *Bioinformatics* **33**: 558-560.
521 Friedman J, Hastie T, Tibshirani R. 2010. Regularization Paths for Generalized Linear Models
522 via Coordinate Descent. *J Stat Softw* **33**: 1-22.
523 Garagnani P, Bacalini MG, Pirazzini C, Gori D, Giuliani C, Mari D, Di Blasio AM, Gentilini D,
524 Vitale G, Collino S et al. 2012. Methylation of ELOVL2 gene as a new epigenetic
525 marker of age. *Aging Cell* **11**: 1132-1134.
526 Gire V, Dulic V. 2015. Senescence from G2 arrest, revisited. *Cell Cycle* **14**: 297-304.
527 Hannum G, Guinney J, Zhao L, Zhang L, Hughes G, Sadda S, Klotzle B, Bibikova M, Fan JB,
528 Gao Y et al. 2013. Genome-wide methylation profiles reveal quantitative views of
529 human aging rates. *Mol Cell* **49**: 359-367.
530 Hanzelmann S, Beier F, Gusmao EG, Koch CM, Hummel S, Charapitsa I, Joussen S, Benes V,
531 Brummendorf TH, Reid G et al. 2015. Replicative senescence is associated with
532 nuclear reorganization and with DNA methylation at specific transcription factor
533 binding sites. *Clin Epigenetics* **7**: 19.
534 Harrison DE, Strong R, Sharp ZD, Nelson JF, Astle CM, Flurkey K, Nadon NL, Wilkinson JE,
535 Frenkel K, Carter CS et al. 2009. Rapamycin fed late in life extends lifespan in
536 genetically heterogeneous mice. *Nature* **460**: 392-395.
537 He S, Sharpless NE. 2017. Senescence in Health and Disease. *Cell* **169**: 1000-1011.
538 Horvath S. 2013. DNA methylation age of human tissues and cell types. *Genome Biol* **14**:
539 R115.
540 Horvath S, Lu AT, Cohen H, Raj K. 2019. Rapamycin retards epigenetic ageing of
541 keratinocytes independently of its effects on replicative senescence, proliferation
542 and differentiation. *Aging (Albany NY)* **11**: 3238-3249.

543 Horvath S, Oshima J, Martin GM, Lu AT, Quach A, Cohen H, Felton S, Matsuyama M, Lowe
544 D, Kabacik S et al. 2018. Epigenetic clock for skin and blood cells applied to
545 Hutchinson Gilford Progeria Syndrome and ex vivo studies. *Aging (Albany NY)* **10**:
546 1758-1775.
547 Horvath S, Raj K. 2018. DNA methylation-based biomarkers and the epigenetic clock theory
548 of ageing. *Nat Rev Genet* **19**: 371-384.
549 Huang da W, Sherman BT, Lempicki RA. 2009. Systematic and integrative analysis of large
550 gene lists using DAVID bioinformatics resources. *Nat Protoc* **4**: 44-57.
551 Kennedy AL, Morton JP, Manoharan I, Nelson DM, Jamieson NB, Pawlikowski JS, McBryan
552 T, Doyle B, McKay C, Oien KA et al. 2011. Activation of the PIK3CA/AKT pathway
553 suppresses senescence induced by an activated RAS oncogene to promote
554 tumorigenesis. *Mol Cell* **42**: 36-49.
555 Kennedy BK, Lamming DW. 2016. The Mechanistic Target of Rapamycin: The Grand
556 ConducTOR of Metabolism and Aging. *Cell Metab* **23**: 990-1003.
557 Levine ME, Lu AT, Quach A, Chen BH, Assimes TL, Bandinelli S, Hou L, Baccarelli AA, Stewart
558 JD, Li Y et al. 2018. An epigenetic biomarker of aging for lifespan and healthspan.
559 *Aging (Albany NY)* **10**: 573-591.
560 Lopez-Otin C, Blasco MA, Partridge L, Serrano M, Kroemer G. 2013. The hallmarks of aging.
561 *Cell* **153**: 1194-1217.
562 Lowe R, Overhoff MG, Ramagopalan SV, Garbe JC, Koh J, Stampfer MR, Beach DH, Rakyan
563 VK, Bishop CL. 2015. The senescent methylome and its relationship with cancer,
564 ageing and germline genetic variation in humans. *Genome Biol* **16**: 194.
565 Lu AT, Quach A, Wilson JG, Reiner AP, Aviv A, Raj K, Hou L, Baccarelli AA, Li Y, Stewart JD et
566 al. 2019. DNA methylation GrimAge strongly predicts lifespan and healthspan.
567 *Aging (Albany NY)* **11**: 303-327.
568 Lucanic M, Lithgow GJ, Alavez S. 2013. Pharmacological lifespan extension of invertebrates.
569 *Ageing Res Rev* **12**: 445-458.
570 Mannick JB, Morris M, Hockey HP, Roma G, Beibel M, Kulmatycki K, Watkins M,
571 Shavlakadze T, Zhou W, Quinn D et al. 2018. TORC1 inhibition enhances immune
572 function and reduces infections in the elderly. *Sci Transl Med* **10**.
573 Marioni RE, Shah S, McRae AF, Chen BH, Colicino E, Harris SE, Gibson J, Henders AK,
574 Redmond P, Cox SR et al. 2015. DNA methylation age of blood predicts all-cause
575 mortality in later life. *Genome Biol* **16**: 25.
576 Martin-Herranz DE, Aref-Eshghi E, Bonder MJ, Stubbs TM, Choufani S, Weksberg R, Stegle
577 O, Sadikovic B, Reik W, Thornton JM. 2019. Screening for genes that accelerate the
578 epigenetic aging clock in humans reveals a role for the H3K36 methyltransferase
579 NSD1. *Genome Biol* **20**: 146.
580 Martin-Montalvo A, Mercken EM, Mitchell SJ, Palacios HH, Mote PL, Scheibye-Knudsen M,
581 Gomes AP, Ward TM, Minor RK, Blouin MJ et al. 2013. Metformin improves
582 healthspan and lifespan in mice. *Nat Commun* **4**: 2192.
583 McCartney DL, Walker RM, Morris SW, McIntosh AM, Porteous DJ, Evans KL. 2016.
584 Identification of polymorphic and off-target probe binding sites on the Illumina
585 Infinium MethylationEPIC BeadChip. *Genom Data* **9**: 22-24.
586 McHugh D, Gil J. 2018. Senescence and aging: Causes, consequences, and therapeutic
587 avenues. *J Cell Biol* **217**: 65-77.
588 Niccoli T, Partridge L. 2012. Ageing as a risk factor for disease. *Curr Biol* **22**: R741-752.

589 Partridge L, Deelen J, Slagboom PE. 2018. Facing up to the global challenges of ageing.
590 *Nature* **561**: 45-56.
591 Pinkston JM, Garigan D, Hansen M, Kenyon C. 2006. Mutations that increase the life span
592 of C. elegans inhibit tumor growth. *Science* **313**: 971-975.
593 Piper MD, Blanc E, Leitao-Goncalves R, Yang M, He X, Linford NJ, Hoddinott MP, Hopfen C,
594 Soultoukis GA, Niemeyer C et al. 2014. A holidic medium for Drosophila
595 melanogaster. *Nat Methods* **11**: 100-105.
596 Pryor R, Norvaisas P, Marinos G, Best L, Thingholm LB, Quintaneiro LM, De Haes W, Esser
597 D, Waschina S, Lujan C et al. 2019. Host-Microbe-Drug-Nutrient Screen Identifies
598 Bacterial Effectors of Metformin Therapy. *Cell* **178**: 1299-1312 e1229.
599 Rae MJ, Butler RN, Campisi J, de Grey AD, Finch CE, Gough M, Martin GM, Vijg J, Perrott
600 KM, Logan BJ. 2010. The demographic and biomedical case for late-life
601 interventions in aging. *Sci Transl Med* **2**: 40cm21.
602 Raj K, Horvath S. 2020. Current perspectives on the cellular and molecular features of
603 epigenetic ageing. *Exp Biol Med (Maywood)* doi:10.1177/1535370220918329:
604 1535370220918329.
605 Reeve A, Simcox E, Turnbull D. 2014. Ageing and Parkinson's disease: why is advancing age
606 the biggest risk factor? *Ageing Res Rev* **14**: 19-30.
607 Saxton RA, Sabatini DM. 2017. mTOR Signaling in Growth, Metabolism, and Disease. *Cell*
608 **168**: 960-976.
609 Selman C, Lingard S, Choudhury AI, Batterham RL, Claret M, Clements M, Ramadani F,
610 Okkenhaug K, Schuster E, Blanc E et al. 2008. Evidence for lifespan extension and
611 delayed age-related biomarkers in insulin receptor substrate 1 null mice. *Faseb J* **22**:
612 807-818.
613 Slack C, Alic N, Foley A, Cabecinha M, Hoddinott MP, Partridge L. 2015. The Ras-Erk-ETS-
614 Signaling Pathway Is a Drug Target for Longevity. *Cell* **162**: 72-83.
615 Sturm G, Cardenas A, Bind MA, Horvath S, Wang S, Wang Y, Hagg S, Hirano M, Picard M.
616 2019. Human aging DNA methylation signatures are conserved but accelerated in
617 cultured fibroblasts. *Epigenetics* doi:10.1080/15592294.2019.1626651: 1-16.
618 Tiku V, Antebi A. 2018. Nucleolar Function in Lifespan Regulation. *Trends Cell Biol* **28**: 662-
619 672.
620 Tomasetti C, Li L, Vogelstein B. 2017. Stem cell divisions, somatic mutations, cancer
621 etiology, and cancer prevention. *Science* **355**: 1330-1334.
622 Wang M, Lemos B. 2019. Ribosomal DNA harbors an evolutionarily conserved clock of
623 biological aging. *Genome Res* **29**: 325-333.
624 Wessells RJ, Fitzgerald E, Cypser JR, Tatar M, Bodmer R. 2004. Insulin regulation of heart
625 function in aging fruit flies. *Nat Genet* **36**: 1275-1281.
626 Wilson BE, Jacob S, Yap ML, Ferlay J, Bray F, Barton MB. 2019. Estimates of global
627 chemotherapy demands and corresponding physician workforce requirements for
628 2018 and 2040: a population-based study. *Lancet Oncol* **20**: 769-780.
629 Yang Z, Wong A, Kuh D, Paul DS, Rakyan VK, Leslie RD, Zheng SC, Widschwendter M, Beck S,
630 Teschendorff AE. 2016. Correlation of an epigenetic mitotic clock with cancer risk.
631 *Genome Biol* **17**: 205.
632 Ye X, Linton JM, Schork NJ, Buck LB, Petrascheck M. 2014. A pharmacological network for
633 lifespan extension in Caenorhabditis elegans. *Aging Cell* **13**: 206-215.
634 Youn A, Wang S. 2018. The MiAge Calculator: a DNA methylation-based mitotic age
635 calculator of human tissue types. *Epigenetics* **13**: 192-206.

636 Zimmermann A, Hofer S, Pendl T, Kainz K, Madeo F, Carmona-Gutierrez D. 2018. Yeast as a
637 tool to identify anti-aging compounds. *FEMS Yeast Res* **18**.
638
639

640

641 **Acknowledgements**

642 IB acknowledges funding from ERC StG 311331, ERC PoC 842174, Royal Society Research Grant,
643 The Bill Lyons foundation. SB acknowledges support from the Wellcome Trust
644 (218274/Z/19/Z). This work was supported in part by the CRUK-UCL Centre Award [C416/A25145]
645 awarded to IB and SB. EJT has been funded by MRC (MR/K501372/1) and BBSRC (BB/P002579/1)
646 and DM is funded by the BBSRC (BB/N503629/1). JG, and MS are supported by U.S. Department of
647 Energy under Contract No. DE-AC02-05CH11231 and the Congressionally Directed Medical
648 Research Programs Breast Cancer Research Program Era of Hope Scholar Award BC141351.

649 **Authors contribution**

650 SB, IB developed initial concept. SB, IB, RL and CLB finalised concept developing and designed
651 experiments. RL, SE and APW analysed data. RL developed the CellAgeClock. CLB and EJT
652 provided cell culture expertise. CL, EJT, ERS, VEMM, DM and IB performed all experiments. SE,
653 SB, IB, RL, CLB wrote the manuscript. JCG and MRS provided critical reagents. All authors
654 discussed results and commented on and approved the manuscript.

655 **Competing interest**

656 The authors declare no competing interest.

657 **Additional information**

658 Correspondence and requests for materials should be addressed to IB, CLB, RL and SB.

659 **Figure Legends**

660 **Figure 1.** Development of CellAgeClock for monitoring subtle ageing difference in cells in culture.
661 A) Predicted age of control samples using three existing epigenetic clocks. Predicted epigenetic
662 age for control samples across all experiments as estimated by the Multi-tissue clock
663 (green), the Skin and Blood clock (orange) and the PhenoAge clock (yellow). Fitted lines are
664 shown with 95% confidence intervals (semi-transparent). All three clocks show a trend to
665 increase in predicted age with progressing passage, however there is considerable
666 variability in predictions, particularly for the PhenoAge clock. The Multi-tissue clock
667 consistently predicted cells to have the highest epigenetic age, while the PhenoAge clock

668 consistently predicted cells to have the lowest epigenetic age, which even reached below
669 zero for several samples at various passages.
670 B) Heatmap representing 23 CpG probes that undergo hypomethylation with increasing cell
671 passage and 19 CpGs that undergo hypermethylation with increasing cell passage. These
672 42 CpG probes were used to develop the CellAgeClock. Probes that undergo
673 hypomethylation and hypermethylation with increasing passage were separated and ordered
674 by their methylation values per row. The mean absolute difference between passage 20 and
675 passage 10 among clock CpGs is 0.2.
676 C) Testing the CellAgeClock on HMF and HDF samples that were not used to train the clock.
677 The gray dashed line represents the diagonal (perfect prediction). The fitted line of the actual
678 data is shown in blue, with a 95% confidence interval (semi-transparent). Cell passages are
679 predicted accurately.
680
681 **Figure 2.** Using the CellAgeClock for the detection of anti-ageing drugs.
682 A) The CellAgeClock predictions of Human Dermal Fibroblasts (HDF) and
683 B) Human Mammary Fibroblasts (HMF). Represented is Predicted-Actual Passage for Passage
684 16, 18 and 20, showing deceleration of the CellAgeClock upon treatment with anti-ageing
685 drugs rapamycin (5nM), Dactolisib/BEZ235 (10nM), torin2 (5nM) and Trametinib (0.1nM).

686
687 **Figure 3.** Treatment with anti-ageing drugs decreases markers of senescence.
688 A) Schematic illustrating the experimental set-up conducted in P10 to P22 HMFs, passaged
689 weekly.
690 B) Multi-parameter analysis of senescence markers. Colour coding used to illustrate the
691 number of Z scores of the experimental drug value from the respective control mean.
692 Scores highlighted in red denote a shift towards a more proliferative phenotype and
693 scores highlighted in green denote a shift to a more senescent phenotype.
694 C) P22 HMFs stained with DAPI (blue) and Cell Mask, p21, p16, IL-6, or nucleolin (red), or
695 SA-β-Gal (blue) following 96-day treatment with 5nM Rapamycin, 10nM
696 Dactolisib/BEZ235, 0.1nM Trametinib or their respective controls. Size bar, 100μm.

697
698 **Figure 4.** Drugs that decelerate the CellAgeClock extend lifespan *in vivo*.
699 A) Lifespan analysis on w^{Dah} background wild type flies fed with SYA food containing different
700 concentration of rapamycin or ethanol as solvent control. For each condition, 150 flies were
701 used.
702 B) Lifespan analysis on w^{Dah} background wild type flies fed with SYA food containing different
703 concentration of Dactolisib/BEZ235 or DMSO as solvent control. For each condition, 150
704 flies were used.

705 C) Lifespan analysis on w^{Dah} background wild type flies fed with SYA food containing different
706 concentration of torin2 or DMSO as solvent control. For each condition, 150 flies were used.
707 D) Schematic representation of our approach combining novel CellAgeClock and other ageing
708 biomarkers *in vitro* primary human cell, together with *in vivo Drosophila* lifespan
709 experiments, for a detailed and robust capture of anti-ageing drug potential.
710

711 **Supplemental Figure Legends**

712 **Supplemental Figure 1.** Drug treatment of HMF did not affect cell growth as measured by
713 population doubling. Represented are population doubling measurements from passage 9
714 to passage 21 for A) rapamycin (5nM), B) trametinib (0.1nM), C) Dactolisib/BEZ235
715 (10nM), D) Torin2 (5nM) and corresponding vehicle controls.

716

717 **Supplemental Figure 2.**

718 A) Scheme for developing of the CellAge clock. A) Primary human mammary fibroblasts
719 and dermal fibroblasts, from passages 10 to 20, were used for CpG methylation
720 profiling and using elastic net regression 42 CpGs were selected to develop the
721 CellAgeClock that predicts cell passage.
722 B) The beanplots showing the overall distribution of DNA methylation values (all CpGs,
723 n=736,001) are presented. Overall DNA methylation levels decrease with increasing
724 cell passage. The lines show where the clock CpGs sit in the distributions (mean per
725 passage group), and are connected across passages to see how their methylation
726 levels change. The plots show the mean methylation changes the clock CpGs are
727 undergoing with increasing passage, separated by those that become hypo- and
728 hypermethylated, in the contextof the global DNA methylation patterns of all CpGs.
729 C) Barplots showing the percentage of CpGs falling into the corresponding genomic
730 feature. Lighter bars show the percentages of clock CpGs (x% of the 42 CpGs). Darker
731 bars show the background distribution (all other CpGs analyzed = 735,959 CpGs).
732 Clock CpGs fall more often into IGRs. Barplots on the left are separated into gene
733 promoters, gene bodies and IGRs for which in the CellAgeClock CpGs we found 12, 14
734 and 16, respectively. More detailed separation of the CellAgeClock CpGs into 5'UTR (2
735 CpGs), TSS200 (1 CpG), TSS1500 (7 CpGs), 1st exon (2 CpGs), gene body (13 CpGs)
736 and 3'UTR (1CpG) and IGR (16 CpG).
737

Supplemental Figure 3. Western blot analysis on HMFs treated with anti-ageing drugs. Western blots were probed for phospho-S6K (Thr 389) showing p85 S6K Thr412 and lower band p70 S6K Thr389, total S6K, phospho-4EBP (Thr37/46), non-phospho-4EBP, pERK (Thr202/Tyr204), total ERK, and H3 as a loading control. Western blots analysis of A) HMF passage 10 and B) HMF passage 14 C) HMF passage 14 only 8h treatment with anti-ageing drugs. The analysis reflect rapid (S6K) and slower (4EBP) decreases in phosphorylation, increased phosphorylation (Akt Ser 473 and Akt Thr308) owing to S6K-IRS negative feedback loop, and resilience to phosphorylation changes owing to pMEK rebound and pERK feedback reactivation.

Supplemental Figure 4.

A) A scatterplot of the cumulative population doubling against the actual passage for control and rapamycin samples.

B) A scatterplot of the cumulative population doubling against the predicted passage from CellAge for control and rapamycin samples.

Supplemental Figure 5. Predicted age of control samples and samples treated with potential anti-ageing drugs using three existing epigenetic clocks.

Predictions of epigenetic age made using the Multi-Tissue (A1-D1, green), Skin & Blood (A2-D2, orange) and PhenoAge (A3-D3, yellow) clocks. Age predictions are indicated for samples treated with rapamycin (A1-A3), Dactolisib/BEZ235 (B1-B3), trametinib (C1-C3), torin2 (D1-D3), as compared with the set of control samples. These comparisons show that the existing clocks do not consistently indicate the anti-ageing effects of these treatments on cultured cells.

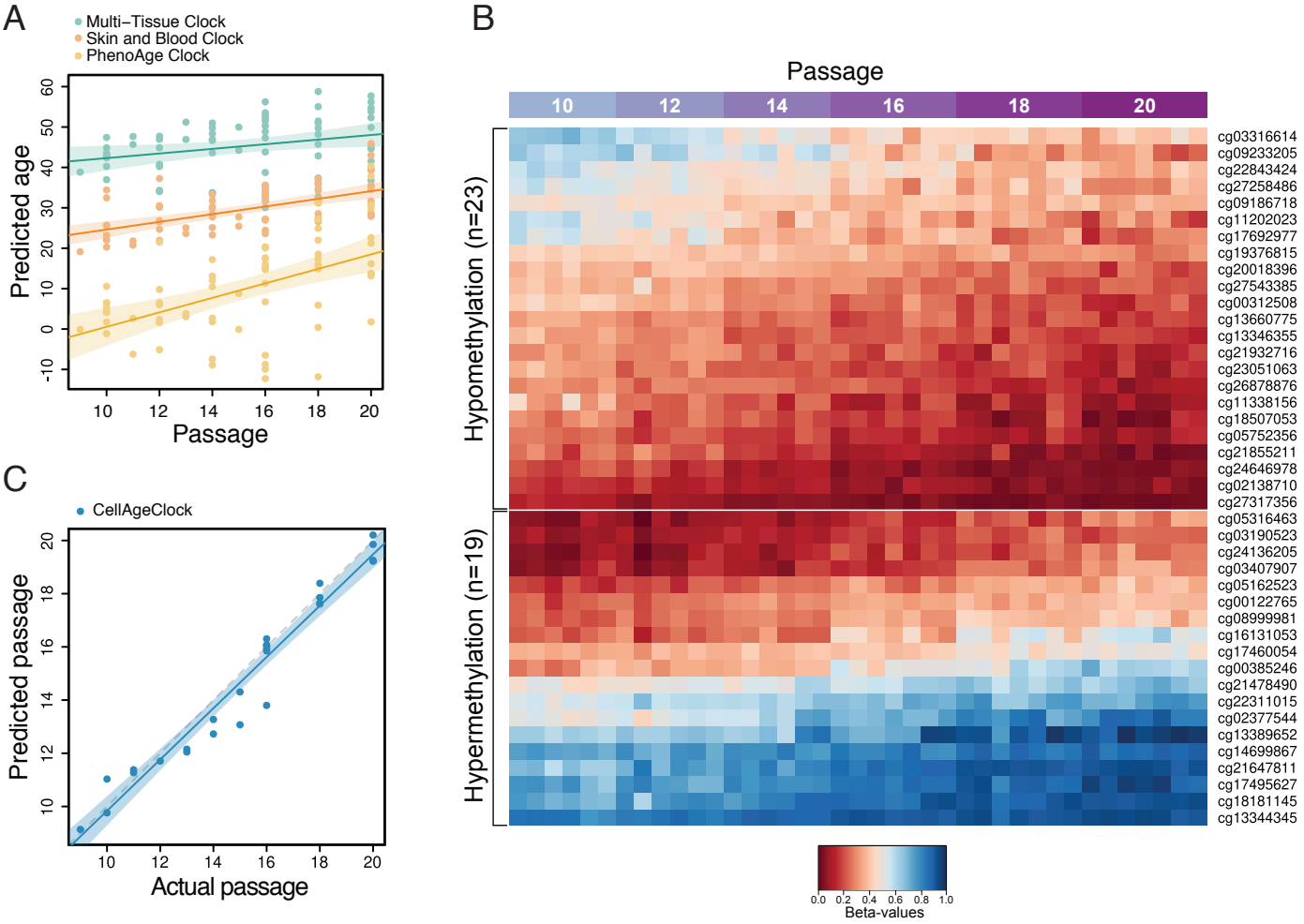
A
Multi−Tissue Clock
Skin and Blood Clock
PhenoAge Clock
Predicted age
Passage
B
Passage
10
12
14
16
18
20
Hypomethylation (n=23)
Hypermethylation (n=19)
cg03316614
cg09233205
cg22843424
cg27258486
cg09186718
cg11202023
cg17692977
cg19376815
cg20018396
cg27543385
cg00312508
cg13660775
cg13346355
cg21932716
cg23051063
cg26878876
cg11338156
cg18507053
cg05752356
cg21855211
cg24646978
cg02138710
cg27317356
cg05316463
cg03190523
cg24136205
cg03407907
cg05162523
cg00122765
cg08999981
cg16131053
cg17460054
cg00385246
cg21478490
cg22311015
cg02377544
cg13389652
cg14699867
cg21647811
cg17495627
cg18181145
cg13344345
0.0 0.2 0.4 0.6 0.8 1.0
Beta-values
C
CellAgeClock
Predicted passage
Actual passage

Figure 1.

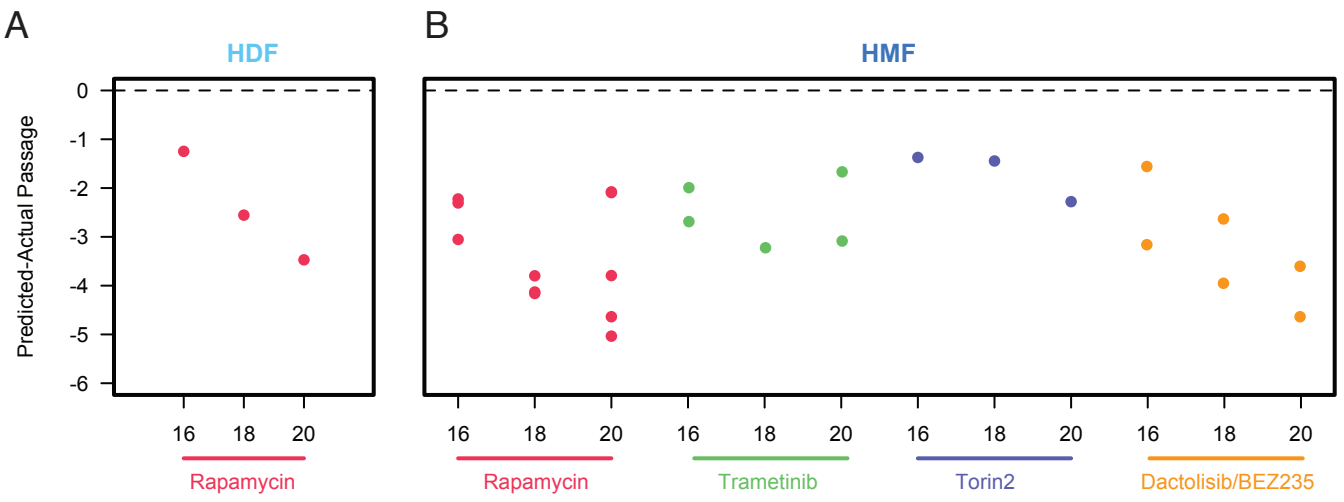
A
HDF
B
HMF
Predicted-Actual Passage
0
-1
-2
-3
-4
-5
-6
16
18
20
Rapamycin
Rapamycin
Trametinib
Torin2
Dactolisib/BEZ235

Figure 2.

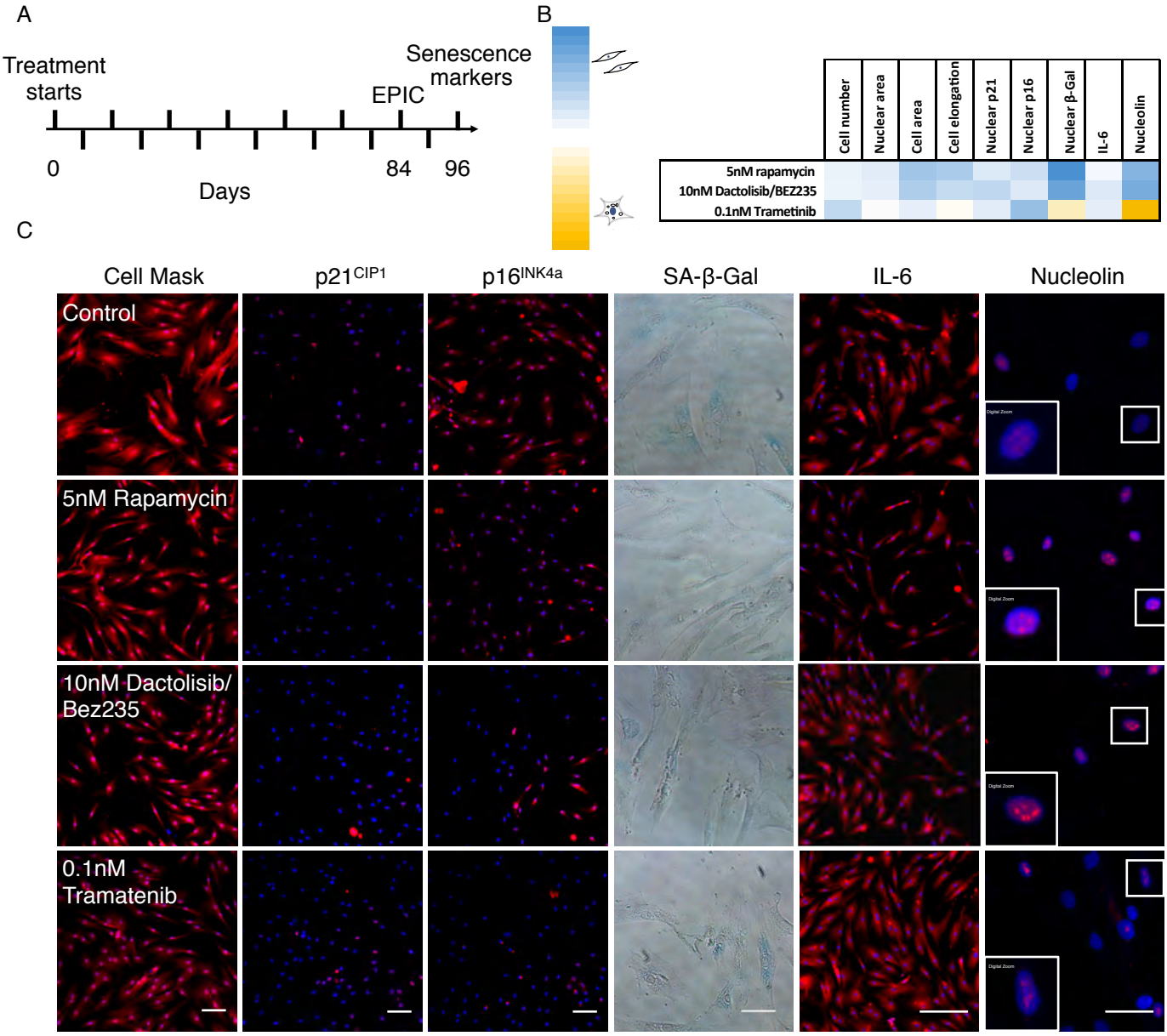
A
Treatment starts
Senescence markers
EPIC
0
84
96
Days
B
Cell number
Nuclear area
Cell area
Cell elongation
Nuclear p21
Nuclear p16
Nuclear β-Gal
IL-6
Nucleolin
5nM rapamycin
10nM Dactolisib/BEZ235
0.1nM Trametinib
C
Cell Mask
p21CIP1
p16INK4a
SA-β-Gal
IL-6
Nucleolin
Control
5nM Rapamycin
10nM Dactolisib/ Bez235
0.1nM Tramatenib

Figure 3

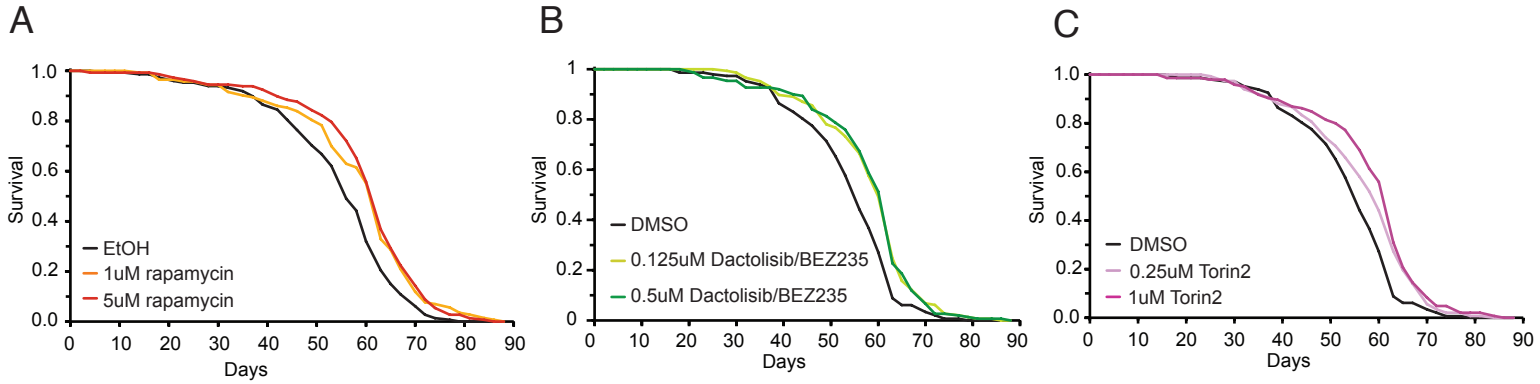
A
Survival
Days
EtOH
1uM rapamycin
5uM rapamycin
B
DMSO
0.125uM Dactolisib/BEZ235
0.5uM Dactolisib/BEZ235
C
DMSO
0.25uM Torin2
1uM Torin2

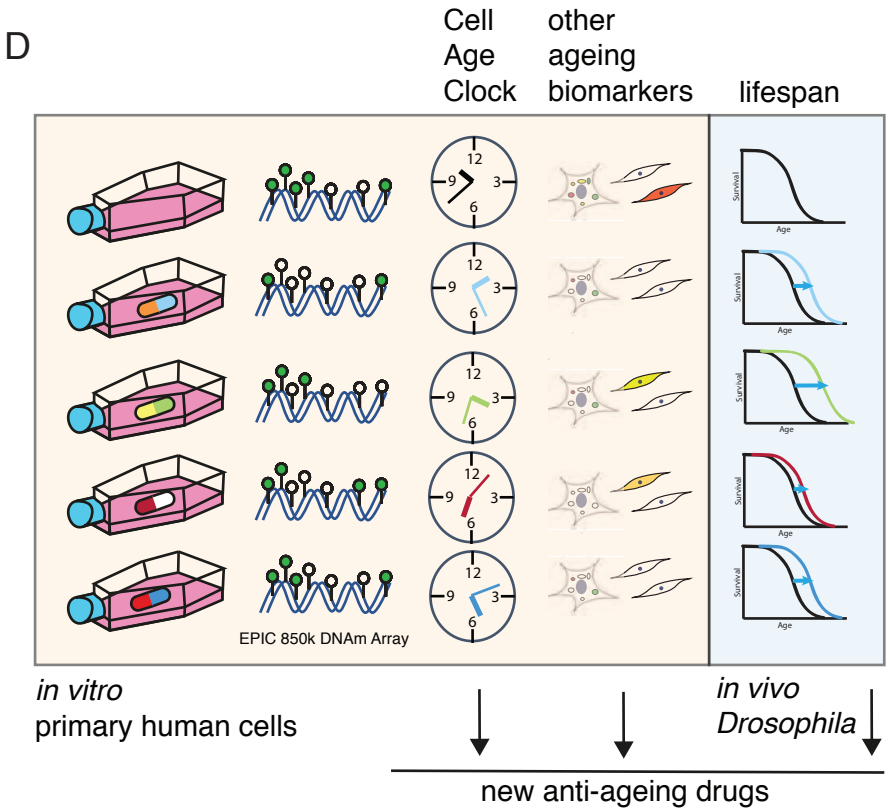
D
Cell Age Clock
other ageing biomarkers
lifespan
EPIC 850k DNAm Array
in vitro
primary human cells
in vivo
Drosophila
new anti-ageing drugs

Figure 4

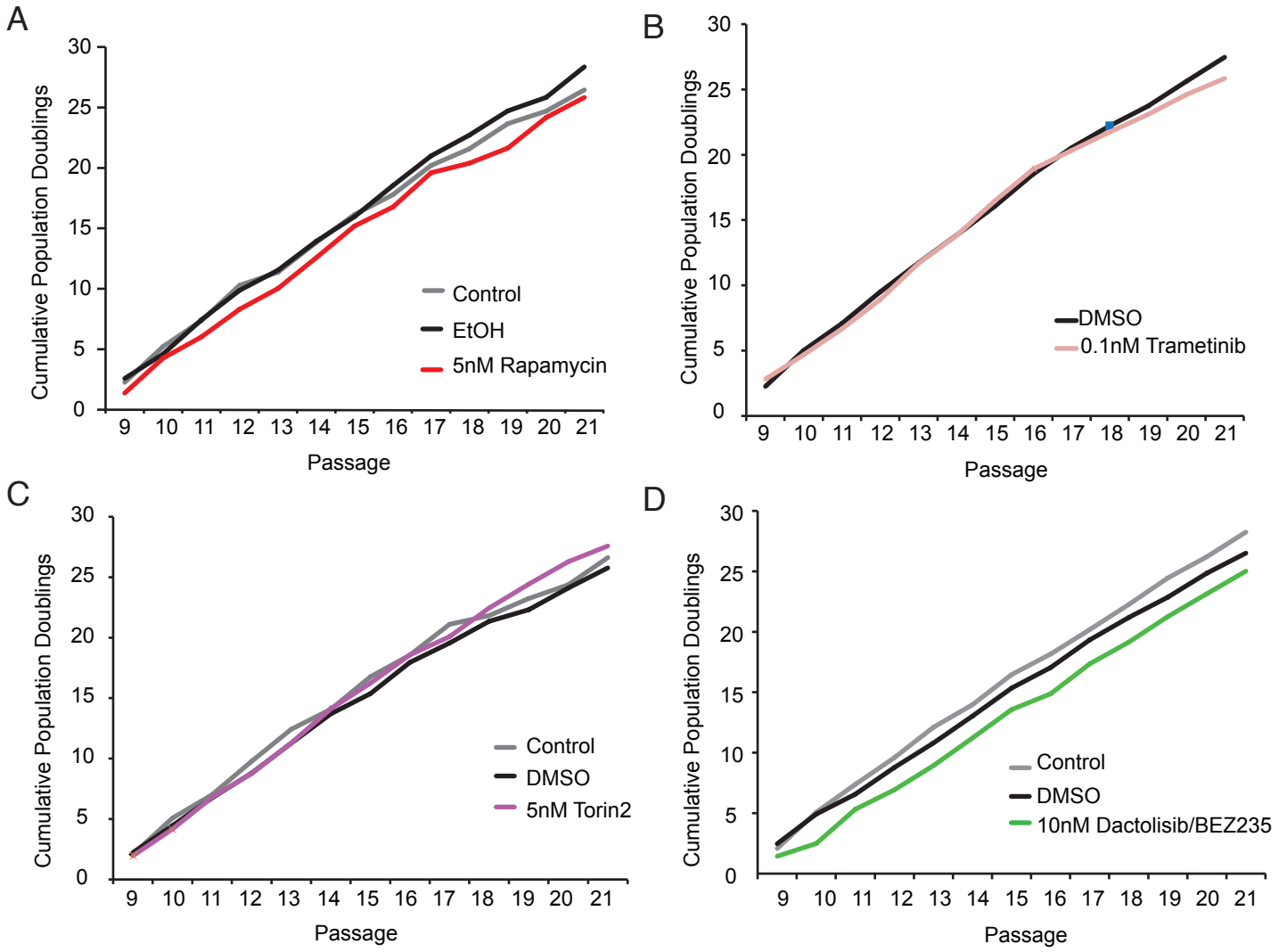

Supplemental Fig.1.

A

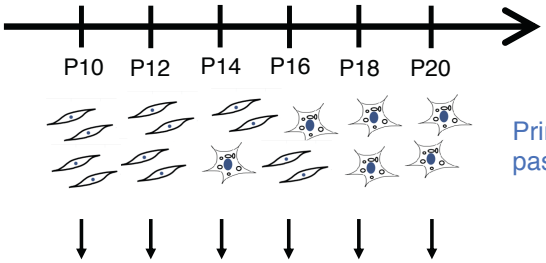

Primary human fibroblasts (HMF and HDF) from passages 10 to 20 were used for CpG methylation profiling.

gDNA, Illumina EPIC CpG methylation platform

Identification CpGs undergoing DNA methylation changes with incresing cell passage using linear regression.

Preselected 2,543 CpGs were used to build the clock model by elastic net regression.

42 CpGs were selected to develop the CellAgeClock that predicts cell passage.

The CellAgeClock was then used on a separate dataset of HMF and HDF samples for the validation of accurate passage prediction and on samples that were treated with anti-ageing drugs.

B

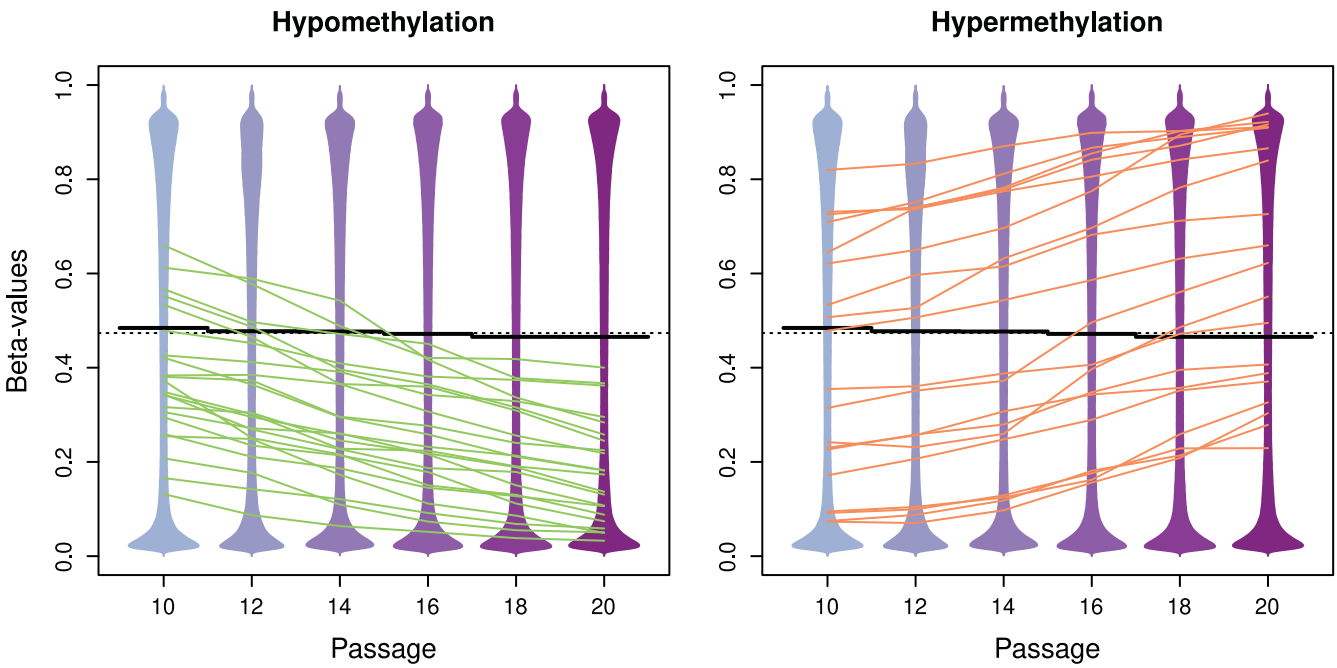

C

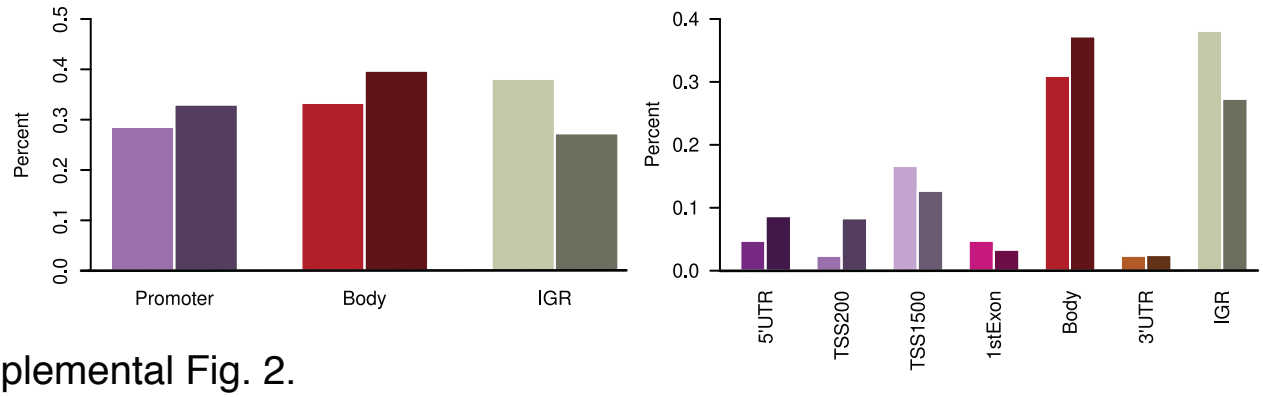

Supplemental Fig. 2.

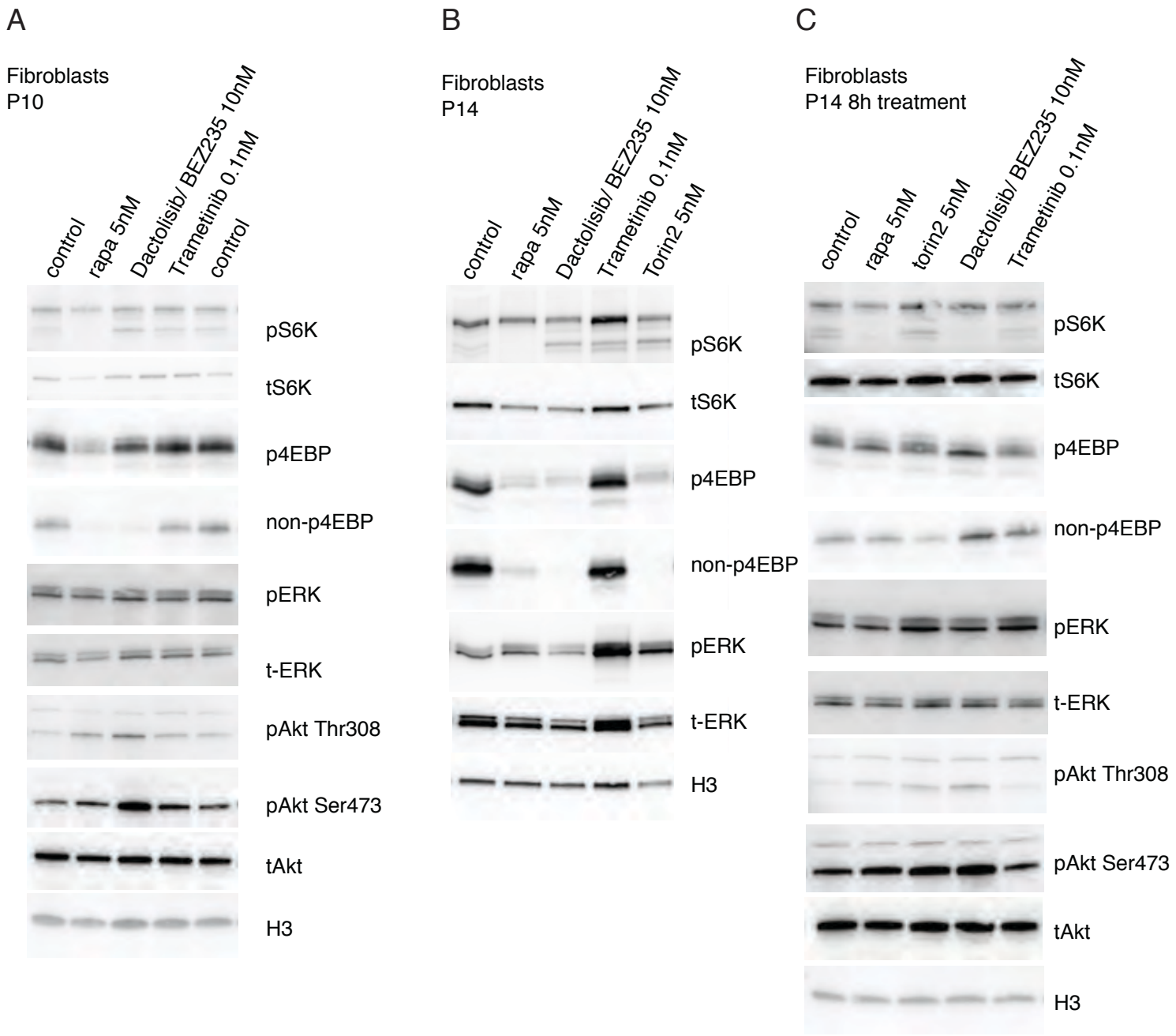

Supplemental Fig. 3

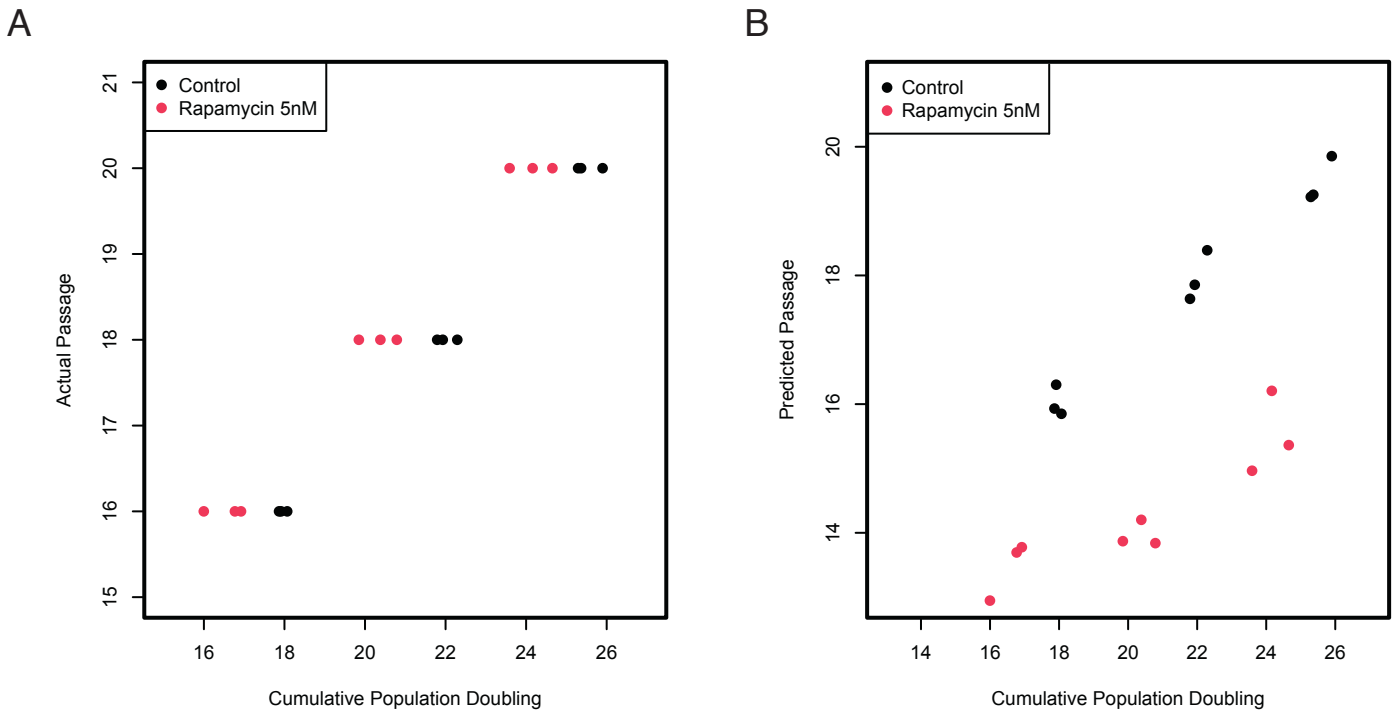

Supplemental Fig. 4.

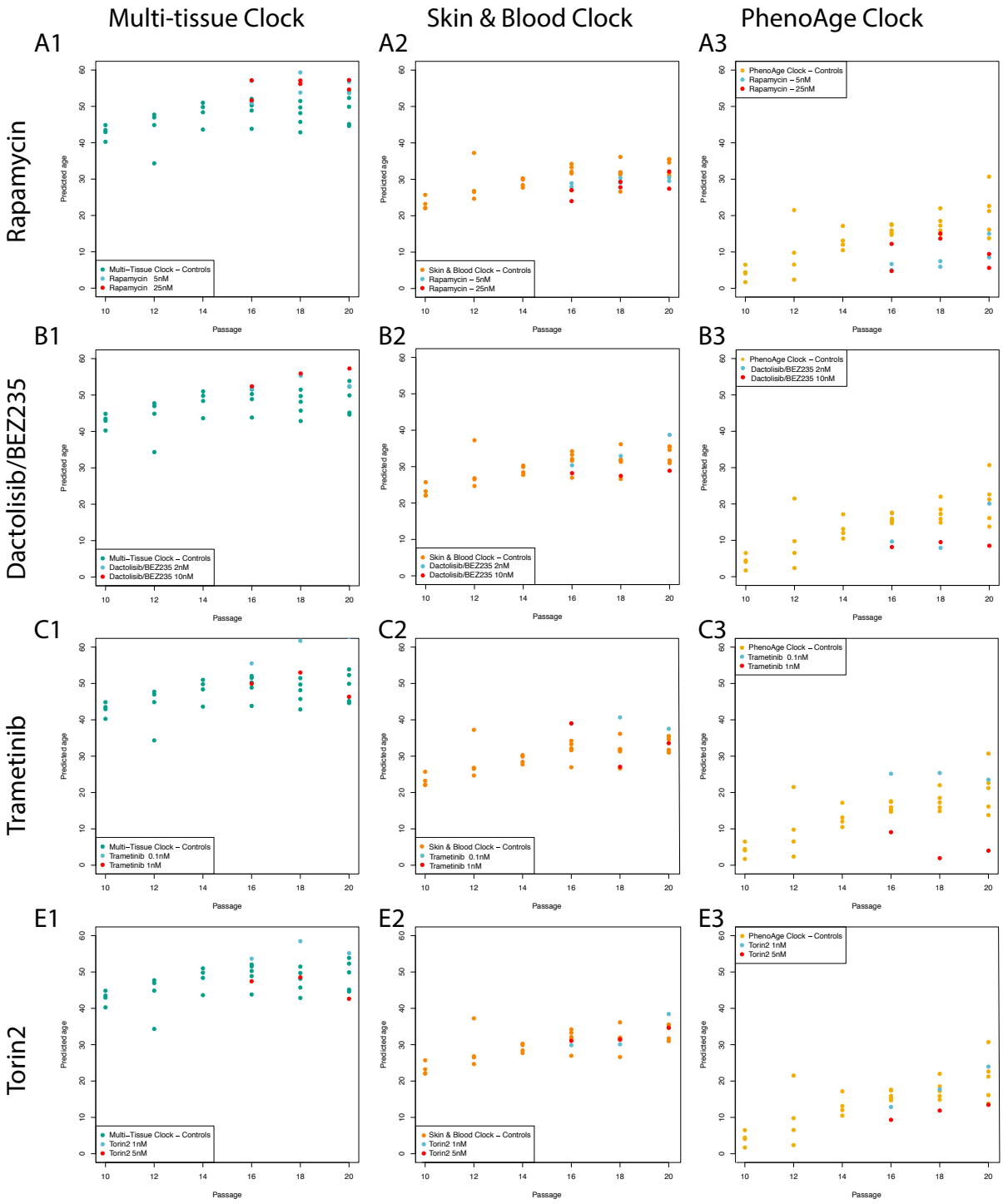

Supplemental Fig. 5